Brain morphometry and longitudinal relaxation time of spontaneously hypertensive rats (SHR) in early and intermediate stages of hypertension investigated by 3D VFA-SPGR MRI

Brain morphometry and longitudinal relaxation time of spontaneously hypertensive rats (SHR) in early and intermediate stages of hypertension investigated by 3D VFA-SPGR MRI

Sunil Koundal[a], Xiaodan Liu[a], Simon Sanggaard[a], Kristian Mortensen[b], Joanna Wardlaw[d], Maiken Nedergaard[b,c], Helene Benveniste[a], Hedok Lee[a]

[a]Department of Anesthesiology, Yale School of Medicine, New Haven, Connecticut

[b]Center for Translational Neuromedicine, Faculty of Health and Medical Sciences, University of Copenhagen, Copenhagen, Denmark

[c]Division of Glia Disease and Therapeutics, Center for Translational Neuromedicine, University of Rochester Medical School, Rochester, New York, USA.

[d]Center for Clinical Brain Sciences, The University of Edinburgh, Edinburgh, UK; UK Dementia Research Institute at The University of Edinburgh, The University of Edinburgh, Edinburgh, UK; Row Fogo Centre for Research into Ageing and the Brain, The University of Edinburgh, Edinburgh, UK.

Address correspondence to

Hedok Lee, PhD
Department of Anesthesiology
Yale School of Medicine
New Haven, CT
hedok.lee@yale.edu

Number of figures/tables: 9/3
Conflict of interest: No authors declare competing financial interests

Abstract

Cerebral small vessel disease(s) (SVD) result from pathological changes of the small blood vessels in the brain and is common in older people. The diagnostic features by which SVD manifests in brain includes white matter hyperintensities, lacunes, dilated perivascular spaces, microbleeds, and atrophy. In the present study, we use *in vivo* MRI to characterize brain morphometry and longitudinal relaxation time (T1) of spontaneously hypertensive rats (SHR) to study the contribution of chronic hypertension to SVD relevant pathology. Male SHR and Wistar-Kyoto (WKY) rats underwent 3D variable flip angle spoiled gradient echo brain MRI at 9.4T at early (7 weeks old) and established (19 weeks old) stages of hypertension. The derived proton density weighted and T1 images were utilized for morphometry and to characterize T1 properties in grey matter, white matter (WM) and cerebrospinal fluid (CSF). Custom tissue probability maps were constructed for accurate computerized whole brain tissue segmentations and voxel-wise analyses. Characteristic morphological differences between the two strains included enlarged ventricles, smaller corpus callosum (CC) volumes and general 'thinning' of CC in SHR compared to WKY rats at both age groups. While we did not observe parenchymal T1 differences, the T1 of CSF was elevated in SHR compared to controls. Collectively these findings indicate that SHR rats develop WM atrophy which is a clinically robust MRI biomarker associated with WM degeneration.

Introduction

Cerebral small vessel disease(s) (SVD) are a group of disorders that result from pathological changes of the small blood vessels in the brain leading to cognitive dysfunction and dementia – referred to as "vascular contribution to cognitive impairment and dementia" or VCID (Gorelick PB et al., 2011;Greenberg SM, 2006;Iadecola C, 2013;Pantoni L, 2010;Wardlaw JM et al., 2013). SVD is the most common cause of vascular dementia in the elderly, affecting 15-20 million people world-wide (Brown R et al., 2018;Kapasi A et al., 2017;Rosenberg GA et al., 2016;Wardlaw JM, et al., 2013). The etiology of sporadic SVD is still not understood and effective pharmacological interventions are yet to be found (Iadecola C, 2013). A significant challenge for clinical studies focused on understanding the underlying cause(s) of SVD relates to the multitude of diagnostic features by which SVD manifests. Hallmark diagnostic criteria for SVD by magnetic resonance imaging (MRI) includes white matter hyperintensities (leukoaraiosis), lacunes, hemorrhages ('microbleeds'), and dilated perivascular spaces. Leukoaraiosis, in particular, is a common feature of SVD and associated with corpus callosum atrophy and VCID in elderly subjects (Ryberg C et al., 2011;Ryberg C et al., 2008).

While several risk factors for sporadic SVD and VCID have been identified including hypertension, smoking, and diabetes (Khan U et al., 2007), their relative importance and mechanistic impact have been difficult to dissect given the variable clinical phenotypes. Small rodent models have been developed to help address the relative impact of the clinically identified SVD risk factors on the disparate disease phenotypes. However, because of the significantly lower white matter (WM) to grey matter (GM) volume ratios in rodents' brain

compared to human brain there are technical challenges in studying WM pathology in the small rodent brain by in vivo MRI.

The spontaneously hypertensive (SHR) rat (Okamoto K and Aoki K, 1963;Smith TL and Hutchins PM, 1979) is a polygenetic inherited primary hypertension model of the equivalent clinical condition and it is a suitable model for studying the contribution of chronic hypertension to SVD pathology. The SHR rat is normotensive at birth and progressively develops hypertension starting around 5-6 weeks of life, reaching a chronic hypertensive state by 24 weeks of age (Pitiot A et al., 2007). The adverse effects of chronic hypertension on brain morphometry in SHR rats have been documented post-mortem by histology (Hong E et al., 1992;Mori S et al., 1995;Sutterer JR et al., 1980;Wyss JM et al., 1992). For example, reduced striatal, cortical and corpus callosum volumes as well as enlarged cerebral ventricles were reported in adult SHRs compared to WKY rats (Amenta F et al., 2003;Huang SM et al., 2016;Sabbatini M et al., 1999;Sabbatini M et al., 2001). A notable and consistent morphological feature of SHRs (but not Wistar-Kyoto (WKY), control rats) is the early onset of cerebral ventricular enlargement which develops spontaneously when they are still only mildly hypertensive and progresses over time (Bendel P and Eilam R, 1992;Pitiot A, et al., 2007;Tajima A et al., 1993). Although post-mortem studies of brain pathology in SHR versus WKY rats support certain clinical features of SVD observed in humans (e.g. brain atrophy) the previous studies in SHR are often limited to a single age group, and morphological changes during early phases of hypertension are rarely reported albeit strong correlations between hypertension, cerebral atrophy and VCID in human have been reported (Jokinen H et al., 2012;Jokinen H et al., 2007;Ryberg C, et al., 2011;Ryberg C, et al., 2008;Salerno JA et al., 1992). MRI studies of SHR

and WKY rats documenting brain morphometric changes have been scarce. Instead, most MRI studies of SHR rats have focused on characterizing changes in cerebral diffusion and cerebral hemodynamics occurring during transition from the pre-hypertensive state to chronic hypertension. For example, a recent diffusion tensor imaging (DTI) study reported progressive diffusion coefficients changes in brain regions associated with executive function before onset of behavioral impairment (Lopez-Gil X et al., 2014). Further, cerebral blood flow (CBF) and blood volume were found to be reduced in young SHR rats, which progressively decrease with aging (Kim T et al., 2014;Li Y et al., 2015). Of note, the diagnostic MRI hallmarks of clinical SVD including WM hyperintensities, progressive development of WM atrophy or enlarged peri-vascular spaces (Dufouil C et al., 2001), which have not been reported in SHR rats.

MR sequences for optimal morphometric characterization of the small rodent brain should be acquired in 3D at high spatial resolution (with adequate signal-to-noise ratios) and with decent tissue contrast-to-noise ratios to accurately discriminate GM, WM and CSF (Gaser C et al., 2012;Meyer CE et al., 2017;Sumiyoshi A et al., 2014). We recently developed a 3D variable flip angle spoiled gradient echo (VFA-SPGR) imaging technique for rodents that provide a whole brain 3D proton density weighted (PDW) image as well as a longitudinal relaxation time (T1) parametric map (Lee H et al., 2018). The 3D PDW image is ideally suited to study morphometry and the T1 parametric map can track pathological tissue degenerations such as white matter hyperintensities. Here we apply this new 3D acquisition paradigm to characterize whole brain morphological and T1 differences between WKY and SHR at two ages (7 and 19 weeks old). The main objectives were to characterize morphometric changes in the pre-

hypertensive period and in an intermediate stage of chronic hypertension with specific focus on white matter pathology given its importance for clinical SVD and VCID.

Methods

Animals

All animal experiments were approved by the local animal welfare authority (Danish Animal Experiments Inspectorate). Seven-week-old (WKY, N=11 body weight: 234 ± 24g male; SHR, N=8 body weight: 218 ± 24g male) and 19-week old (WKY, N=7 body weight: 366 ± 9g male; SHR, N=8 body weight: 341 ± 31g male) old WKY and SHR rats were obtained from Charles River, Germany. Up to 5-6 weeks old, SHR rats are 'pre-hypertensive' and by 14 weeks they rapidly develop a systolic blood pressure increase of up to 200-220 mmHg, therefore the two age groups studied here represent early hypertension and an intermediate stage of chronic hypertension. Both SHR and WKY were fed with the same basic diet with a normal levels of salt content.

MRI parameters

All MRI acquisitions were performed on a Bruker 9.4T/30 magnet (Bruker BioSpin, Billerica MA) with a BGA-12SHP imaging gradient system interfaced to an Avance III console controlled by Paravision 5.1 software. A volume transmit radio frequency (RF) with an inner diameter of 11.2 cm and a 4-channel phase array RF receiver head coil were employed for signal generation and reception, respectively. All animals were anesthetized with dexmedetomidine (0.015-0.020 mg/kg/hr) delivered via a subcutaneous catheter placed in the

flank supplemented with 0.6-1.0 % isoflurane delivered in a 1:1 Air:O_2 mixture and allowed to breathe spontaneously in the supine position. Physiological parameters including respiratory rate, oxygen saturation, body temperature, and heart rate were continuously monitored using MRI compatible monitors (SA Instruments, Inc., Stony Brook, NY) and maintained within normal physiological ranges during the scans as previously described (Benveniste H et al., 2017).

The MR imaging protocol comprises a quantitative 3D T1 mapping technique using the VFA-SPGR 3D T1 mapping technique as described previously (Lee H, et al., 2018). By performing a set of spoiled gradient echo sequence at multiple flip angles, T1 can be calculated from a canonical linear relationship between detected signals and scanner parameters. However, VFA-SPGR is known to yield erroneous T1 due to the spatial inhomogeneity profile of the RF transmit (B1+) coil which depends on the dielectric constant, electrical conductivity, and magnetic susceptibility. We have previously shown that VFA-SPGR sequence with the B1+ correction yields accurate and reliable T1 across the entire brain. Following an anatomical localizer scan, B1+ map was acquired using the double angle method and rapid acquisition with relaxation enhancement (RARE) sequence at two excitation flip angles (TR/TE/FA/NEX=10000 msec/22 msec/70°,140°/1, 0.24x0.24x0.40 mm acquisition time=10 min 40 sec). Subsequently, acquisition of the VFA-SPGR scan was taken at 6 flip angles at fixed TR (TR/TE/FA/NEX=15 msec/4 msec/2°~30°/1, 0.24x0.24x0.26 mm, acquisition time=24 min 30sec) and the VFA-SPGR signals were fitted with linear least square fit with B1+ correction to yield 3D PDW and quantitative T1 maps.

MRI image analyses

Morphometric differences between SHR and WKY rats were investigated using whole brain voxel-wise analysis to detect regional morphological differences and a semi-automated computerized method to estimate the corpus callosum volumes. 3D PDW images calculated from the parametric T1 maps were analyzed by voxel-wise deformation-based morphometry (DBM) using the SPM12 (http://www.fil.ion.ucl.ac.uk/spm) software package. Intensity inhomogeneity in PDWs caused by the RF receive array coil was corrected by the N4 algorithm (Tustison NJ et al., 2010) and then segmented into GM, WM and CSF compartments using the unified segmentation algorithm (Ashburner J and Friston KJ, 2005). Visual inspection of the PDW segmentation into the three tissue compartments using the publicly available Wistar rat template (Valdes-Hernandez PA et al., 2011) revealed gross underestimation of the CSF compartment, mostly in lateral ventricles where CSF was misclassified as GM or WM as shown in Fig. 1. Underestimation of CSF was consistently observed irrespective of age and strain and the error became more pronounced in aged SHR rats. Because the DARTEL spatial registration algorithm derives the deformation fields from these erroneously segmented images the accuracy of the registration and deformation fields in the ensuing analysis will be compromised. We therefore manually edited the population averaged GM, WM and CSF images to assign misclassified tissue to the proper tissue compartment, and the new custom-designed WKY-SHR tissue probability maps greatly improved the accuracy of the CSF segmentation as shown in Fig. 1.

The segmented images were then utilized to derive the voxel-wise deformation fields between individual scans and the population averaged template created by means of the DARTEL spatial registration algorithm (Ashburner J, 2007). The resulting deformation fields

were further processed to calculate the voxel-wise Jacobian determinant, which reveals volumetric expansions or contractions between the individual brain scans and the group averaged template (Chung MK et al., 2001;Thompson PM et al., 2000). The Jacobian maps were smoothed by isotropic 0.6mm full width half maximum Gaussian smoothing kernel. Regional morphological differences between WKY and SHR rats were statistically analyzed by a t-test in the framework of general linear modelling with the total intracranial volume (TIV) as a covariate.

Calculations of the corpus callosum (CC) volumes from each animal were performed by a semi-automated computerized method. Following the GM, WM, and CSF segmentations as described in the voxel-wise analysis, the animals were divided into four groups, separated by strain and age, and spatially normalized to the corresponding groups only, to derive age and strain specific templates. CC was then manually delineated in each of the four group templates as binary masks and the total volume of CC of each animal was calculated by taking the sum of all Jacobian determinants within the masks multiplied by the volume of corresponding CC masks in the templates. The age and strain specific registration technique is a time-efficient strategy, because it bypasses the laborious manual delineation of the CC in each animal while at the same time reducing potential misregistrations between the groups (WKY vs SHR). Finally, the thickness of CC was estimated for the CC masks in the templates using the thickness measurement algorithm (Hildebrand T and Ruegsegger P, 1997) implemented in Amira 6.5 visualization and quantitative analysis software (Thermo Fisher Scientific, Waltham, MA, USA). Strategies for achieving blinding among the MRI data among analysts were not practical because ventricular dilation in SHR rats was a highly robust phenotype when compared to WKY rats.

The T1 maps were also analyzed using the whole brain voxel-wise analysis approach to detect regional T1 differences and the semi-automated computerized method to estimate the T1 of CC as a whole. In the whole brain voxel-wise analysis, T1 maps were spatially normalized by applying the deformation fields derived from the morphological analysis onto the corresponding T1 maps followed by Gaussian smoothing kernel of 0.6mm and the t-test implemented in GLM without any covariate. To calculate T1 within CC, CC masks and deformation fields derived from the semi-computerized methods in the morphological study were applied onto corresponding T1 maps and subsequently, the mean and standard deviation (SD) of T1 in each animal were calculated.

Results

Following the image segmentation using the new WKY-SHR tissue probability maps, total GM, WM and CSF volumes were calculated for each animal as summarized in Table 1. Statistical analyses of the brain volumes were performed using a 2-way ANOVA with strain (WKY vs SHR) and age (7 vs 19 weeks) as main effects. In all of the three tissue compartments along with TIV, significant effects of the strain and age ($F(1, 30)$ $p < 0.002$) were found. As shown, WKY rats' tissue volumes increased by 3 % (GM), 16 % (WM), 10 % (CSF) and 8 % (TIV) with aging but none of the tissue compartments yielded significant interactions effect between strain and age. In SHR rats tissue volumes increased by 5 % (GM), 14 % (WM), 33 % (CSF) and 10 % (TIV) with age; with no significant interaction effects. Normalizing GM, WM, and CSF volumes by TIV, as shown in Table 1, revealed significant effects of the strain on WM and CSF volumes ($F(1, 30)$ $p < 0.001$) and the effect of age was significant with respect to GM and WM

but not CSF. Again, none of the tissue compartments yielded significant interaction effects. Pearson's correlations between body weights and the TIVs were significant as shown in Fig. 2. and the linear regression lines indicated a constant offset in y-intercept between the two strains.

Voxel-wise DBM analyses were performed to characterize morphological differences between WKY and SHR rats in the 7 and 19 weeks old age groups. In Fig. 3, parametric maps (t-values) calculated from the general linear model were converted into p-values, uncorrected for multiple comparisons, and overlaid onto a population averaged WKY-SHR PDW image to display areas of significant morphological differences. At both age groups, enlargement of the CSF compartment including the lateral ventricles and aqueduct was a characteristic phenotype of young SHR rats compared to WKY rats, and this trait became more pronounced at 19 weeks. Tissue areas with larger tissue volumes in WKY rats compared to SHR rats at 7 weeks included midbrain, thalamus and lateral preoptic area. At 19 weeks, tissue regions with larger volume in WKY compared to SHR rats included midbrain, thalamus, corpus callosum, preoptic and regions associated with the basal ganglia. Importantly, in 19 weeks old SHR rats, significant WM volume loss in the splenium of corpus callosum was observed, which was absent in young, 7 weeks old SHR rats. Morphological changes in SHR rats from 7 to 19 weeks old were also computed using DBM as shown in Fig. 4. Visual cortex volume was found to be significantly larger in 7-week-old rats compared to 19-week-old rats in both strains. In WKY rats, the midbrain, thalamus, and corpus callosum volumes were larger in 19-week-old rats when compared to 7-week-old. In SHR rats, midbrain and ventricles enlarged while cortical volumes were reduced from 7 to 19 weeks old.

Volumetric differences between WKY and SHR in the corpus callosum were further validated by the semi-automated computerized technique. Manually delineated CC binary masks were superimposed onto the strain and age specific population averaged PDW images as shown in Fig. 5. SHR templates exhibited progressively enlarged lateral ventricles and subtle enlargement of the frontal horn of the lateral ventricles compared to WKY rats. The CC volumes calculated from the semi-automated technique are summarized in Table 2 and statistical analyses on CC volume differences were performed using a 2-way ANOVA with strain (WKY vs SHR) and age (7 vs 19 weeks) as main effects. The main effects of strain and age were significantly different ($F(1, 30)$, $p < 0.001$) even after accounting for the TIV differences. No significant interaction with aging was found. To test whether the observed volumetric differences were due in part to differences in CC thickness, the thickness distributions and thickness maps were also calculated as shown in Fig. 6. In WKY rats, thickening of the CC as a function of aging was observed as a shift in the entire histogram profiles in the direction of thickening, which was also supported by the color-coded thickness maps. Between WKY and SHR rats, the percent relative frequency of CC thickness above 0.8 mm was consistently higher in WKY compared to SHR irrespective of the age and the percent frequency of thinner regions (less than 0.5 mm) was consistently higher in SHR rats.

T1 map analyses comprised whole brain global analysis, voxel-wise comparisons to detect regional T1 differences, and T1s within the CC using the strain and age specific CC masks as shown in Fig. 5. In the global whole brain analysis, the mean and SD of T1s calculated within GM and WM tissue compartments are summarized in Table 3 and analyzed by a 2-way ANOVA with strains (WKY vs SHR) and age (7 vs 19 weeks) as main effects. No statistical differences

were found in T1 of GM and WM but T1 of CSF ($F(1,30)=29.95$, $p<0.001$) was significantly different (increased in SHR rats) between the two strains, and significant effect of aging was found in WM ($F(1,30)=6.36$, $p=0.017$) and CSF ($F(1,30)=5.46$, $p=0.026$). No interaction between the strains and age were found. In the voxel-wise analysis, individual T1maps were spatially normalized using the deformation fields derived from the morphological analyses and Fig. 7 shows the population averaged T1 maps for each strain at the two age groups. Visual inspection of the T1 maps did not detect focal conspicuous lesions, indicative of WM hyperintensities. While the spatial registration steps substantially reduced the size of lateral ventricles in the SHR rats to match across the two strains, imperfect registrations were still discernable at the tissue-CSF boundaries as shown Fig. 8. As seen from Fig. 7, the lateral ventricles were markedly larger in SHR compared to WKY rats even after the spatial normalization. Interestingly in the regions far from the boundaries where partial volume effect is absent (i.e. middle of ventricles), the CSF T1 was significantly different between the strains. In the direction of T1 being lower in WKY compared to SHR, no regional differences were found. In the ROI analyses, no statistical differences in aging or interaction but significant effect of strain ($F(1,30)=6.08$, $p=0.020$) was found where T1 of SHR was 3% higher than WKY as summarized in Table 3. Finally. we extracted T1 within the focal regions of the splenium of CC that was morphologically smaller (lower averaged Jacobian) in SHR compared to WKY rats as shown in Fig. 9. The average and SD of the Jacobian within the focal splenium regions were 1.046 ± 0.043 (WKY 7weeks), 1.129 ± 0.042 (WKY 19weeks), 0.869 ± 0.060 (SHR 7weeks), and 0.929 ± 0.034 (SHR 19weeks) and the 2-way ANOVA yielded statistical differences in the main effect of strain ($F(1,30)=145.8$, $p<0.0001$) and age ($F(1,30)=21.09$, $p<0.0001$) but the interaction was not significant. Similarly, average and SD

of T1s within the focal splenium regions were 1950 ± 84 msec (WKY 7 weeks), 1885 ± 85 msec (WKY 19 weeks), 1940 ± 44 msec (SHR 7 weeks), and 1877 ± 95 msec (SHR 19 weeks) as shown in Fig. 9 and the statistical differences were found only for the main effect of age ($F(1,30)=5.17$, $p<0.03$).

Discussion

The present study focused on the characterization of differences in brain morphometry and longitudinal relaxation time between WKY and SHR rats during the early and intermediate stages of (chronic) hypertension. Morphological characterization is of importance because it is proven to be a sensitive diagnostic marker for the staging of SVD in humans and it is therefore a reliable platform to assess the clinical relevance of any of the pertinent 'SVD' animal models such as the SHR rats. While studies have reported on morphological differences between the SHR and WKY rats in the past, most of these studies were performed ex-vivo with fixative preservatives which are known to collapse ventricles and shrink anatomical tissue volumes to varying degrees (Ma Y et al., 2008). To our knowledge only one other study (Pitiot A, et al., 2007) which applied in-vivo morphological MRI compared 12 weeks old SHR and Brown Norway rats, however, Brown Norway rats are not of a same genetic origin as SHR and it is unclear if the observed differences were due to strain or blood pressure differences. Our study supplement and further validate the previous in vivo MRI data by comparing SHR rat's brain morphometry to their parent strain, the WKY rats, in addition to investigating the cerebral effects of aging as well as hypertension.

The acquisition of high resolution 3D anatomical MR images in the small rodent brain in vivo poses technical challenges in regard to achieving both superior contrast-to-noise and signal-to-noise ratios to resolve tissue structures (Sawiak SJ et al., 2009), while also maintaining a reasonable scan time. The commonly applied T2W RARE sequence requires several hours of scan time and potential head and body movements during the scans may corrupt the data, adding RF induced heating, and prolonged anesthesia/sedation is not ideal for animals with significant morbidity such as chronic hypertension (Ma Y, et al., 2008;Valdes-Hernandez PA, et al., 2011). By using our new VFA-SPGR imaging technique, we were able to substantially reduce scan time to less than an hour while still attaining good tissue contrast as shown in the 3D PDW images which were used for morphometric analysis. We note that the scan time can be reduced even further by taking only a low flip angle SPGR image for the acquisition of the 3D PDW image (and skip the T1 map) for studies focused solely on morphometry.

Morphometric analyses were performed by calculating total brain/tissue volumes, voxel-wise volumetric analysis, and CC volumes. Total brain/tissue volume analysis is used to detect gross volumetric differences between strains and proven to be a sensitive diagnostic imaging marker of aging and hypertension related structural change in humans (Good CD et al., 2001;Salerno JA, et al., 1992;Verdelho A et al., 2010;Wiseman RM et al., 2004). We used computerized whole brain segmentation to create custom WKY-SHR tissue probability maps which greatly improved the accuracy of the tissue segmentation quality as other studies have also suggested (Dodero L et al., 2013;Meyer CE, et al., 2017;Tucci V et al., 2014). The custom WKY-SHR tissue probability maps were crucial to reveal that GM, WM, and CSF volumes were all significantly lower in SHR compared to WKY rats irrespective of age, extending the finding of

a previous study reporting smaller TIVs in SHR rats compared to WKY rats in much older rats (35 weeks old) (Kaiser D et al., 2014). Further by normalizing the tissue compartment volumes to TIV we were able to document significant effects of the strain type on WM and CSF volumes and, in addition, we documented that GM and WM (but not CSF) volumes were age-dependent, and these results emphasize the importance of considering TIVs as a confounding factor when comparing morphological differences between the strains across multiple age groups.

Since the body weights of the SHR were lower than age-matched WKY rats, we also evaluated the relationship between body weights and TIVs similar to the correlations found in humans with gender and TIVs (Gur RC et al., 1999;Luders E et al., 2005;Nopoulos P et al., 2000). Indeed, significant correlations between TIVs and body weights were documented, and linear regression analyses revealed that TIVs of SHR were consistently lower than WKYs across ages. Therefore, smaller TIV in SHR rats is a trait unrelated to the status of chronic hypertension.

Voxel-wise volumetric analysis revealed that significant morphological differences between the two strains were evident as early as 7 weeks of age and became more extensive at 19 weeks. In SHR rats a pre-hypertensive, early stage hypertensive stage and later-stage hypertension are present at 5-weeks, 10-weeks and 15 weeks, respectively (Hom S et al., 2007). At 7-weeks of age the SHR rats in our study are in the early stage of hypertension with a mean blood pressure in the range of 110-120mmHg which is higher when compared to age-matched WKY control rats. Thus, although the younger SHR rats have not yet reached an established chronic hypertensive stage we attribute the very early signs of WM atrophy observed in the SHR rats at 7-weeks to the elevated blood pressure. However, there is a gap in knowledge regarding very early brain morphometry changes during early pre-hypertensive stage in SHR

rats and more studies are needed to fully characterize the genetic trait of SHRs at both pre and post hypertensive stages.

Anatomical regions where SHR rats exhibit smaller tissue volumes compared to WKY rats included midbrain, thalamus, corpus callosum, preoptic, and striatum and these results are consistent with previous studies performed histologically (Nelson DO and Boulant JA, 1981;Ritter S et al., 1988;Tajima A, et al., 1993). In addition, we observed reduced tissue volumes in somatosensory, auditory and insular cortices at 19 weeks compared to 7 weeks old SHR rats. Studies have shown that these areas also exhibit reduced neuronal density in SHR compared to WKY rats (Nelson DO and Boulant JA, 1981). Smaller tissue volume together with reduced neuronal density infer that the total number of neurons is also lower in SHR than WKY rats. The mechanisms underlying brain atrophy in the SHR rats may be related to cerebrovascular changes, perivascular inflammation, dysfunctional cerebrospinal fluid transport and or blood brain barrier compromise (Kaiser D, et al., 2014;Mestre H et al., 2018;Rajani RM et al., 2018).

Ventricular enlargement is a well-documented morphological feature of SHR rats and is an insignificant feature before 4 weeks of age but develops rather abruptly between 4 and 8 weeks of age and thereafter progresses, though at a slower rate, throughout adult life while maintaining normal intraventricular pressure, intracranial pressure and CSF production rate, all of which are consistent with our observation in morphological differences in SHR at two groups (Griswold WR et al., 1981;Naessens DMP et al., 2018;Ritter S, et al., 1988). Cerebral ventricular enlargement is also independent of elevated blood pressure because anti-hypertensive treatment by captopril treatment still resulted in the ventriculomegaly despite improvement in

behavioral tests (Ritter S, et al., 1988;Wyss JM, et al., 1992). Involvement of glycoproteins of the Reissner's fiber has been suggested as a molecular mechanism behind the progressive ventricular dilation but it is still unclear how it is related to aging and ventricular dilation (Martinez-Pena y Valenzuela I et al., 2006). Furthermore, a recent study showed that even normotensive WKY exhibits progressive ventricular dilation with aging (Bors L et al., 2018) and it is plausible that cerebral ventricle enlargement in SHR is accelerated with aging compared to WKY.

Voxel-wise analysis revealed a significantly smaller volume of the splenium of the CC in SHR compared to WKY rats, which was also confirmed by the ROI analysis. Our results support previous histological evidence reporting smaller WM volumes in SHR compared to WKY including anterior commissure, corpus callosum and internal capsule among 3-9 months old SHR (Kaiser D, et al., 2014;Nelson DO and Boulant JA, 1981;Tajima A, et al., 1993). Reduced CC volumes in SHR attributed to the thinning of CC has not been reported previously. Unlike, volume measurement, thickness measures are a widely used diagnostic measure to assess morphometric differences in both clinical and pre-clinical studies because it is independent of confounding factors like TIV (Egaas B et al., 1995). We observed that the thickness and volume of the CC in both strains were age-dependent, and genu and splenium were visibly thinner in SHR compared to WKY rats at both ages. We speculate that the intermediate stage of hypertension hindered the normal growth of CC and the splenium appears to be especially vulnerable. Clinical studies previously reported that the splenium of the CC is indeed particularly vulnerable to hypertension, i.e. an elevated mean diffusivity (MD) and reduced fractional anisotropy (FA) were observed among hypertensive subjects compared to

normotensive controls and both variables were significantly correlated with the cognitive performance and modified by aging (Gons RA et al., 2012;Kennedy KM and Raz N, 2009).

We used quantitative 3D T1 maps to examine T1 changes in the brains of SHR compared to WKY rats. Chronic arterial hypertension in SHR rats causes remodeling of the cerebral vasculature. Several studies have documented cerebral arterial hypertrophy and smooth muscle cell hyperplasia as well as reduction of the luminal diameter of small penetrating arteries, which are all well-described physiological strategies initiated to protect the brain from high perfusion pressures. However, the hypertension-induced vascular remodeling may limit the brain vessels' capacity to dilate thereby increasing the risk of developing hypo-perfusion and ischemia (which can be severe in white matter due to oligodendrocyte death and degeneration of myelinated fibers) (Barry DI and Lassen NA, 1984;Heagerty AM et al., 1993;Jalal FY et al., 2012;Sabbatini M, et al., 2001). Studies have shown that WM pathology in SHR rats dominates and includes vacuolization, de-myelination, significant myelin loss in CC and disarrangement of nerve fibers, and in deep grey matter astrogliosis and microglial activation prevalent (Kaiser D, et al., 2014;Nelson DO and Boulant JA, 1981). These pathological features of untreated SHR rats can also be observed in WMH lesions in humans. In humans WMH lesions by MRI exhibit elevated MD, reduced FA, and elevated T1 (Firbank MJ et al., 2003;Maniega SM et al., 2015;Munoz Maniega S et al., 2017). The elevated T1 observed in WMH lesions in human SVD is interesting because it is suggestive of edema and it has been utilized to identify the pathophysiological changes within normal appearing white matter (NAWM) (Bastin ME et al., 2002;Maniega SM, et al., 2015). We used quantitative T1 maps in the SHR rat study to test its potential utility in detecting similar observations in WM as is observed in SVD patients.

In our study T1 values in both GM and WM were highly consistent between animals with coefficients of variance of 2-3%. Aging from 7 to 19 weeks reduced the T1 which can be attributed to continued growth of WM structures through myelination as reported in humans (Yeatman JD et al., 2014). The comparison of T1 between WKY and SHR rats in GM and WM did not reach statistically significant differences in any of the analyses: global analysis, region of interest in CC and voxel-wise analysis. We were surprised by the lack of T1 changes in the CC since previous studies have reported changes in blood brain permeability (BBB) and diffusion changes in CC of SHR rats compared to controls (Kaiser D, et al., 2014;Lopez-Gil X, et al., 2014). Whole brain wide voxel-wise was also performed to reveal focal changes, and we detected significant differences between SHR and WKY at the tissue-CSF boundaries susceptible to misregistration. We, therefore, conclude that there were no differences in tissue T1's between WKY and SHR at both age groups. However, future studies incorporating larger sample sizes should be explored for potential detection of small T1 differences. These results have implications in studying CBF between SHR and WKY rats when using the arterial spin labelling technique, which requires knowledge of tissue T1 because alterations of the T1 introduce bias in CBF quantification (Kim SG, 1995). Previous studies have assumed T1 of SHR rats to be within a normal value and our study confirms that this assumption is valid (Kim T, et al., 2014;Li Y, et al., 2015). A longitudinal DTI study in SHR and WKY reported significant reduction in FA and elevated MD in CC in SHR compared to WKY implying that the T1 would be elevated in the CC (Lopez-Gil X, et al., 2014) which is contrary to the results of our study. CC is a structure surrounding the lateral ventricles and prone to partial volume effects and may therefore artificially elevate diffusion coefficients at the boundaries and small inclusions of CSF may skew

FA and MD values. Alternatively, the diffusion sequence may be more sensitive in detecting WM changes (compared to T1 mapping) as was previously reported (Firbank MJ, et al., 2003;Wardlaw JM et al., 2009) and more studies are needed to further validate and compare the sensitivity of diffusion and T1 imaging techniques for this purpose.

We observed a significantly higher T1 of CSF (within the center of the lateral ventricles) in SHR rats compared to WKY rats which was intriguing. This observation might be attributed to differences in oxygen tension, temperature, and/or protein constituents within the CSF compartment or all three (Zaharchuk G et al., 2005). Oxygen tension in CSF is governed by the supply of freely diffusible oxygen across the blood-CSF barrier and lower oxygen tension results in higher T1 due to the paramagnetic property of oxygen. CSF oxygen tension is a reflection of the blood oxygenation level in brain parenchyma and if the elevated T1 in CSF in SHR rats was due to higher oxygen tension in CSF we would expect to observe alterations in parenchymal T1 as well (Haddock B et al., 2013;Mehemed TM et al., 2014;Remmele S et al., 2013). Alternatively, CSF protein content might be different between the strains. There are few reports on varying protein CSF profiles between WKY and SHR rats. One study (Gonzalez-Marrero I et al., 2013) reported lower levels of proteins and related this with the (dys)function of blood-CSF barrier (Transthyretin) in SHR compared to WKY. The same study also reported higher levels of blood plasma proteins (IgG, albumin and haptoglobin) and the proteins related with inflammation as a consequence of a leaky blood-CSF barrier in SHR. Another study (Carmona-Calero EM et al., 2013) reported higher levels of P73 protein, which is related to adult neurogenesis, in SHR compared to WKY rats. With increase in total protein concentrations, T1 is, however, expected to decrease which is in contrast with our observation of elevated T1 in SHR compared to WKY

(Yilmaz A et al., 2004). Therefore, it is unlikely that observed T1 differences are due to the differences in total protein concentrations.

Limitations of our study

Some limitations exist in our study. First, animals were not studied longitudinally, but cross-sectionally and the different ages of rats are separate groups. A longitudinal study design with multiple time points from pre-hypertensive till the advanced stage of chronic hypertension could potentially improve sensitivity of the MR parameters in detecting hypertension related morphological and pathological changes. Second, the present study only focused on MR imaging as a diagnostic technique and histology was not performed as it has been done extensively in the past. Third, we did not assess MRI defined morphometry and T1 changes at the 'endstage' of hypertension in old (12-18 month) SHR rats. Finally, although SHR and WKY rats had originated from the same outbred colony, genetic studies have shown substantial differences in the DNA profiles between the two strains (Nabika T et al., 1991;Zhang-James Y et al., 2013). WKY rats were used in this study as a control since it is still genetically the closest normotensive counterpart of SHR rats.

Conclusions

In conclusion, the current study presented a new MRI based methodological approach to analyze both morphometry and T1 using a single imaging method (VFA-SPGR) to characterize morphological differences between WKY and SHR at the two stages of hypertension, and at the same time evaluate T1 changes. Proton density weighted image derived from the 3D VFA-SPGR

sequence yielded sufficiently good signal and contrast to noise ratios to accurately segment GM, WM and CSF using the custom tissue probability maps. Morphometric analyses revealed enlarged ventricles in SHR rats, a well-known morphological trait, and more importantly smaller WM volumes even after considering TIV differences. Semi-computerized CC segmentation method further corroborated this finding and the progressive thinning of the CC in SHR was detected in the anatomical regions known to be vulnerable to damage among SVD patients. The T1 analyses did not reveal significant differences between the strains in brain parenchyma but interestingly a significant difference was found in CSF. To summarize the SHR rats develop WM atrophy which is a clinically robust MRI biomarker associated with WM abnormalities.

Acknowledgements

The present work was supported by National Institutes of Health RF-AG053991, RF-AG057705, R01-NS100366, and Foundation Leducq Transatlantic Network of Excellence (16/CVD/05). A portion of this work was presented at the 26th and 27th Annual Meeting of the International Society for Magnetic Resonance in Medicine.

Figure legends

Figure. 1

Spatially normalized and population averaged CSF compartments were superimposed onto the population averaged proton density weighted image, separated by the strain (WKY vs SHR) and age groups (7 weeks old vs 19 weeks old). CSF compartments segmented by using the publicly available Wistar rat tissue probability maps are shown at top. CSF compartments segmented by the custom made WKY-SHR tissue probability maps are shown at bottom. Color maps indicate CSF probability density.

Figure.2

Total intracranial volumes (TIV) plotted as a function of body weights. Dotted lines represent fitted linear regression lines for WKY (red) and SHR (blue).

Figure.3

Voxel-wise deformation based morphometry analyses comparing WKY and SHR at 7 and 19 weeks old. Statistical significance levels (uncorrected p-values) were superimposed onto the population averaged proton density weighted image.

Figure.4

Voxel-wise deformation based morphometry analyses comparing at 7 and 19 weeks old in WKY and SHR separately. Statistical significance levels (uncorrected p-values) were superimposed onto the population averaged proton density weighted image

Figure.5

Manually delineated corpus callosum masks (red) are superimposed onto strain and age specific population averaged proton density weighted images.

Figure.6

(Top) Thickness maps of corpus callosum for WKY and SHR at the two age groups. Corresponding thickness histograms for 7 weeks (bottom left) and 19 weeks old (bottom right) WKY (red) and SHR (blue).

Figure.7

Population averaged T1 maps for WKY and SHR at 7 and 19 weeks old.

Figure.8

Voxel-wise T1 analyses comparing WKY and SHR at 7 and 19 weeks old. Statistical significance levels (uncorrected p-values) are superimposed onto the population averaged proton density weighted image.

Figure. 9

Averaged and SD of Jacobian (left) and T1 (right) within the focal region of corpus callosum found to be significantly smaller (shown in red) in SHR compare to WKY at 19 weeks old as shown in Fig. 3.

References

Amenta F, Di Tullio MA, Tomassoni D (2003), Arterial hypertension and brain damage--evidence from animal models (review). Clin Exp Hypertens 25:359-380.

Ashburner J (2007), A fast diffeomorphic image registration algorithm. Neuroimage 38:95-113.

Ashburner J, Friston KJ (2005), Unified segmentation. Neuroimage 26:839-851.

Barry DI, Lassen NA (1984), Cerebral blood flow autoregulation in hypertension and effects of antihypertensive drugs. J Hypertens Suppl 2:S519-526.

Bastin ME, Sinha S, Whittle IR, Wardlaw JM (2002), Measurements of water diffusion and T1 values in peritumoural oedematous brain. Neuroreport 13:1335-1340.

Bendel P, Eilam R (1992), Quantitation of ventricular size in normal and spontaneously hypertensive rats by magnetic resonance imaging. Brain Res 574:224-228.

Benveniste H, Lee H, Ding F, Sun Q, Al-Bizri E, Makaryus R, Probst S, Nedergaard M, et al. (2017), Anesthesia with Dexmedetomidine and Low-dose Isoflurane Increases Solute Transport via the Glymphatic Pathway in Rat Brain When Compared with High-dose Isoflurane. Anesthesiology 127:976-988.

Bors L, Toth K, Toth EZ, Bajza A, Csorba A, Szigeti K, Mathe D, Perlaki G, et al. (2018), Age-dependent changes at the blood-brain barrier. A Comparative structural and functional study in young adult and middle aged rats. Brain Res Bull 139:269-277.

Brown R, Benveniste H, Black SE, Charpak S, Dichgans M, Joutel A, Nedergaard M, Smith KJ, et al. (2018), Understanding the role of the perivascular space in cerebral small vessel disease. Cardiovasc Res.

Carmona-Calero EM, Castaneyra-Ruiz L, Gonzalez-Toledo JM, de Paz-Carmona H, Brage C, Castaneyra-Ruiz A, Rancel-Torres MN, Gonzalez-Marrero I, et al. (2013), The expression

of p73 in the organum vasculosum of the lamina terminalis and choroid plexus of spontaneously hypertensive rats. Histol Histopathol 28:925-932.

Chung MK, Worsley KJ, Paus T, Cherif C, Collins DL, Giedd JN, Rapoport JL, Evans AC (2001), A unified statistical approach to deformation-based morphometry. Neuroimage 14:595-606.

Dodero L, Damiano M, Galbusera A, Bifone A, Tsaftsaris SA, Scattoni ML, Gozzi A (2013), Neuroimaging evidence of major morpho-anatomical and functional abnormalities in the BTBR T+TF/J mouse model of autism. PLoS One 8:e76655.

Dufouil C, de Kersaint-Gilly A, Besancon V, Levy C, Auffray E, Brunnereau L, Alperovitch A, Tzourio C (2001), Longitudinal study of blood pressure and white matter hyperintensities: the EVA MRI Cohort. Neurology 56:921-926.

Egaas B, Courchesne E, Saitoh O (1995), Reduced size of corpus callosum in autism. Arch Neurol 52:794-801.

Firbank MJ, Minett T, O'Brien JT (2003), Changes in DWI and MRS associated with white matter hyperintensities in elderly subjects. Neurology 61:950-954.

Gaser C, Schmidt S, Metzler M, Herrmann KH, Krumbein I, Reichenbach JR, Witte OW (2012), Deformation-based brain morphometry in rats. Neuroimage 63:47-53.

Gons RA, van Oudheusden LJ, de Laat KF, van Norden AG, van Uden IW, Norris DG, Zwiers MP, van Dijk E, et al. (2012), Hypertension is related to the microstructure of the corpus callosum: the RUN DMC study. J Alzheimers Dis 32:623-631.

Gonzalez-Marrero I, Castaneyra-Ruiz L, Gonzalez-Toledo JM, Castaneyra-Ruiz A, de Paz-Carmona H, Castro R, Hernandez-Fernaud JR, Castaneyra-Perdomo A, et al. (2013), High

blood pressure effects on the blood to cerebrospinal fluid barrier and cerebrospinal fluid protein composition: a two-dimensional electrophoresis study in spontaneously hypertensive rats. Int J Hypertens 2013:164653.

Good CD, Johnsrude IS, Ashburner J, Henson RN, Friston KJ, Frackowiak RS (2001), A voxel-based morphometric study of ageing in 465 normal adult human brains. Neuroimage 14:21-36.

Gorelick PB, Scuteri A, Black SE, Decarli C, Greenberg SM, Iadecola C, Launer LJ, Laurent S, et al. (2011), Vascular contributions to cognitive impairment and dementia: a statement for healthcare professionals from the american heart association/american stroke association. Stroke 42:2672-2713.

Greenberg SM (2006), Small vessels, big problems. N Engl J Med 354:1451-1453.

Griswold WR, Viney J, Mendoza SA, James HE (1981), Intracranial pressure monitoring in severe hypertensive encephalopathy. Crit Care Med 9:573-576.

Gur RC, Turetsky BI, Matsui M, Yan M, Bilker W, Hughett P, Gur RE (1999), Sex differences in brain gray and white matter in healthy young adults: correlations with cognitive performance. J Neurosci 19:4065-4072.

Haddock B, Larsson HB, Hansen AE, Rostrup E (2013), Measurement of brain oxygenation changes using dynamic T(1)-weighted imaging. Neuroimage 78:7-15.

Heagerty AM, Aalkjaer C, Bund SJ, Korsgaard N, Mulvany MJ (1993), Small artery structure in hypertension. Dual processes of remodeling and growth. Hypertension 21:391-397.

Hildebrand T, Ruegsegger P (1997), Quantification of Bone Microarchitecture with the Structure Model Index. Comput Methods Biomech Biomed Engin 1:15-23.

Hom S, Fleegal MA, Egleton RD, Campos CR, Hawkins BT, Davis TP (2007), Comparative changes in the blood-brain barrier and cerebral infarction of SHR and WKY rats. Am J Physiol Regul Integr Comp Physiol 292:R1881-1892.

Hong E, Ibarra M, Meneses A, Ransanz V, Castillo C (1992), Effects of hypertension and ageing on vascular reactivity and associative learning. Proc West Pharmacol Soc 35:183-185.

Huang SM, Wu YL, Peng SL, Peng HH, Huang TY, Ho KC, Wang FN (2016), Inter-Strain Differences in Default Mode Network: A Resting State fMRI Study on Spontaneously Hypertensive Rat and Wistar Kyoto Rat. Sci Rep 6:21697.

Iadecola C (2013), The pathobiology of vascular dementia. Neuron 80:844-866.

Jalal FY, Yang Y, Thompson J, Lopez AC, Rosenberg GA (2012), Myelin loss associated with neuroinflammation in hypertensive rats. Stroke 43:1115-1122.

Jokinen H, Lipsanen J, Schmidt R, Fazekas F, Gouw AA, van der Flier WM, Barkhof F, Madureira S, et al. (2012), Brain atrophy accelerates cognitive decline in cerebral small vessel disease: the LADIS study. Neurology 78:1785-1792.

Jokinen H, Ryberg C, Kalska H, Ylikoski R, Rostrup E, Stegmann MB, Waldemar G, Madureira S, et al. (2007), Corpus callosum atrophy is associated with mental slowing and executive deficits in subjects with age-related white matter hyperintensities: the LADIS Study. J Neurol Neurosurg Psychiatry 78:491-496.

Kaiser D, Weise G, Moller K, Scheibe J, Posel C, Baasch S, Gawlitza M, Lobsien D, et al. (2014), Spontaneous white matter damage, cognitive decline and neuroinflammation in middle-aged hypertensive rats: an animal model of early-stage cerebral small vessel disease. Acta Neuropathol Commun 2:169.

Kapasi A, DeCarli C, Schneider JA (2017), Impact of multiple pathologies on the threshold for clinically overt dementia. Acta Neuropathol 134:171-186.

Kennedy KM, Raz N (2009), Pattern of normal age-related regional differences in white matter microstructure is modified by vascular risk. Brain Res 1297:41-56.

Khan U, Porteous L, Hassan A, Markus HS (2007), Risk factor profile of cerebral small vessel disease and its subtypes. J Neurol Neurosurg Psychiatry 78:702-706.

Kim SG (1995), Quantification of relative cerebral blood flow change by flow-sensitive alternating inversion recovery (FAIR) technique: application to functional mapping. Magn Reson Med 34:293-301.

Kim T, Richard Jennings J, Kim SG (2014), Regional cerebral blood flow and arterial blood volume and their reactivity to hypercapnia in hypertensive and normotensive rats. J Cereb Blood Flow Metab 34:408-414.

Lee H, Mortensen K, Sanggaard S, Koch P, Brunner H, Quistorff B, Nedergaard M, Benveniste H (2018), Quantitative Gd-DOTA uptake from cerebrospinal fluid into rat brain using 3D VFA-SPGR at 9.4T. Magn Reson Med 79:1568-1578.

Li Y, Shen Q, Huang S, Li W, Muir ER, Long JA, Duong TQ (2015), Cerebral angiography, blood flow and vascular reactivity in progressive hypertension. Neuroimage 111:329-337.

Lopez-Gil X, Amat-Roldan I, Tudela R, Castane A, Prats-Galino A, Planas AM, Farr TD, Soria G (2014), DWI and complex brain network analysis predicts vascular cognitive impairment in spontaneous hypertensive rats undergoing executive function tests. Front Aging Neurosci 6:167.

Luders E, Narr KL, Thompson PM, Woods RP, Rex DE, Jancke L, Steinmetz H, Toga AW (2005), Mapping cortical gray matter in the young adult brain: effects of gender. Neuroimage 26:493-501.

Ma Y, Smith D, Hof PR, Foerster B, Hamilton S, Blackband SJ, Yu M, Benveniste H (2008), In Vivo 3D Digital Atlas Database of the Adult C57BL/6J Mouse Brain by Magnetic Resonance Microscopy. Front Neuroanat 2:1.

Maniega SM, Valdes Hernandez MC, Clayden JD, Royle NA, Murray C, Morris Z, Aribisala BS, Gow AJ, et al. (2015), White matter hyperintensities and normal-appearing white matter integrity in the aging brain. Neurobiol Aging 36:909-918.

Martinez-Pena y Valenzuela I, Carmona-Calero EM, Perez-Gonzalez H, Ormazabal-Ramos C, Fernandez-Rodriguez P, Gonzalez-Marrero I, Castaneyra-Perdomo A, Ferres-Torres R (2006), Alterations of the cerebrospinal fluid proteins and subcommissural organ secretion in the arterial hypertension and ventricular dilatation. A study in SHR rats. Histol Histopathol 21:179-185.

Mehemed TM, Fushimi Y, Okada T, Yamamoto A, Kanagaki M, Kido A, Fujimoto K, Sakashita N, et al. (2014), Dynamic oxygen-enhanced MRI of cerebrospinal fluid. PLoS One 9:e100723.

Mestre H, Tithof J, Du T, Song W, Peng W, Sweeney AM, Olveda G, Thomas JH, et al. (2018), Flow of cerebrospinal fluid is driven by arterial pulsations and is reduced in hypertension. Nat Commun 9:4878.

Meyer CE, Kurth F, Lepore S, Gao JL, Johnsonbaugh H, Oberoi MR, Sawiak SJ, MacKenzie-Graham A (2017), In vivo magnetic resonance images reveal neuroanatomical sex

differences through the application of voxel-based morphometry in C57BL/6 mice. Neuroimage 163:197-205.

Mori S, Kato M, Fujishima M (1995), Impaired maze learning and cerebral glucose utilization in aged hypertensive rats. Hypertension 25:545-553.

Munoz Maniega S, Chappell FM, Valdes Hernandez MC, Armitage PA, Makin SD, Heye AK, Thrippleton MJ, Sakka E, et al. (2017), Integrity of normal-appearing white matter: Influence of age, visible lesion burden and hypertension in patients with small-vessel disease. J Cereb Blood Flow Metab 37:644-656.

Nabika T, Nara Y, Ikeda K, Endo J, Yamori Y (1991), Genetic heterogeneity of the spontaneously hypertensive rat. Hypertension 18:12-16.

Naessens DMP, de Vos J, VanBavel E, Bakker E (2018), Blood-brain and blood-cerebrospinal fluid barrier permeability in spontaneously hypertensive rats. Fluids Barriers CNS 15:26.

Nelson DO, Boulant JA (1981), Altered CNS neuroanatomical organization of spontaneously hypertensive (SHR) rats. Brain Res 226:119-130.

Nopoulos P, Flaum M, O'Leary D, Andreasen NC (2000), Sexual dimorphism in the human brain: evaluation of tissue volume, tissue composition and surface anatomy using magnetic resonance imaging. Psychiatry Res 98:1-13.

Okamoto K, Aoki K (1963), Development of a strain of spontaneously hypertensive rats. Jpn Circ J 27:282-293.

Pantoni L (2010), Cerebral small vessel disease: from pathogenesis and clinical characteristics to therapeutic challenges. Lancet Neurol 9:689-701.

Pitiot A, Pausova Z, Prior M, Perrin J, Loyse N, Paus T (2007), Magnetic resonance imaging as a tool for in vivo and ex vivo anatomical phenotyping in experimental genetic models. Hum Brain Mapp 28:555-566.

Rajani RM, Quick S, Ruigrok SR, Graham D, Harris SE, Verhaaren BFJ, Fornage M, Seshadri S, et al. (2018), Reversal of endothelial dysfunction reduces white matter vulnerability in cerebral small vessel disease in rats. Sci Transl Med 10.

Remmele S, Sprinkart AM, Muller A, Traber F, von Lehe M, Gieseke J, Flacke S, Willinek WA, et al. (2013), Dynamic and simultaneous MR measurement of R1 and R2* changes during respiratory challenges for the assessment of blood and tissue oxygenation. Magn Reson Med 70:136-146.

Ritter S, Dinh TT, Stone S, Ross N (1988), Cerebroventricular dilation in spontaneously hypertensive rats (SHRs) is not attenuated by reduction of blood pressure. Brain Res 450:354-359.

Rosenberg GA, Wallin A, Wardlaw JM, Markus HS, Montaner J, Wolfson L, Iadecola C, Zlokovic BV, et al. (2016), Consensus statement for diagnosis of subcortical small vessel disease. J Cereb Blood Flow Metab 36:6-25.

Ryberg C, Rostrup E, Paulson OB, Barkhof F, Scheltens P, van Straaten EC, van der Flier WM, Fazekas F, et al. (2011), Corpus callosum atrophy as a predictor of age-related cognitive and motor impairment: a 3-year follow-up of the LADIS study cohort. J Neurol Sci 307:100-105.

Ryberg C, Rostrup E, Sjostrand K, Paulson OB, Barkhof F, Scheltens P, van Straaten EC, Fazekas F, et al. (2008), White matter changes contribute to corpus callosum atrophy in the elderly: the LADIS study. AJNR Am J Neuroradiol 29:1498-1504.

Sabbatini M, Baldoni E, Cadoni A, Vitaioli L, Zicca A, Amenta F (1999), Forebrain white matter in spontaneously hypertensive rats: a quantitative image analysis study. Neurosci Lett 265:5-8.

Sabbatini M, Strocchi P, Vitaioli L, Amenta F (2001), Microanatomical changes of intracerebral arteries in spontaneously hypertensive rats: a model of cerebrovascular disease of the elderly. Mech Ageing Dev 122:1257-1268.

Salerno JA, Murphy DG, Horwitz B, DeCarli C, Haxby JV, Rapoport SI, Schapiro MB (1992), Brain atrophy in hypertension. A volumetric magnetic resonance imaging study. Hypertension 20:340-348.

Sawiak SJ, Wood NI, Williams GB, Morton AJ, Carpenter TA (2009), Voxel-based morphometry in the R6/2 transgenic mouse reveals differences between genotypes not seen with manual 2D morphometry. Neurobiol Dis 33:20-27.

Smith TL, Hutchins PM (1979), Central hemodynamics in the developmental stage of spontaneous hypertension in the unanesthetized rat. Hypertension 1:508-517.

Sumiyoshi A, Taki Y, Nonaka H, Takeuchi H, Kawashima R (2014), Regional gray matter volume increases following 7days of voluntary wheel running exercise: a longitudinal VBM study in rats. Neuroimage 98:82-90.

Sutterer JR, Perry J, DeVito W (1980), Two-way shuttle box and lever-press avoidance in the spontaneously hypertensive and normotensive rat. J Comp Physiol Psychol 94:155-163.

Tajima A, Hans FJ, Livingstone D, Wei L, Finnegan W, DeMaro J, Fenstermacher J (1993), Smaller local brain volumes and cerebral atrophy in spontaneously hypertensive rats. Hypertension 21:105-111.

Thompson PM, Giedd JN, Woods RP, MacDonald D, Evans AC, Toga AW (2000), Growth patterns in the developing brain detected by using continuum mechanical tensor maps. Nature 404:190-193.

Tucci V, Kleefstra T, Hardy A, Heise I, Maggi S, Willemsen MH, Hilton H, Esapa C, et al. (2014), Dominant beta-catenin mutations cause intellectual disability with recognizable syndromic features. J Clin Invest 124:1468-1482.

Tustison NJ, Avants BB, Cook PA, Zheng Y, Egan A, Yushkevich PA, Gee JC (2010), N4ITK: improved N3 bias correction. IEEE Trans Med Imaging 29:1310-1320.

Valdes-Hernandez PA, Sumiyoshi A, Nonaka H, Haga R, Aubert-Vasquez E, Ogawa T, Iturria-Medina Y, Riera JJ, et al. (2011), An in vivo MRI Template Set for Morphometry, Tissue Segmentation, and fMRI Localization in Rats. Front Neuroinform 5:26.

Verdelho A, Madureira S, Moleiro C, Ferro JM, Santos CO, Erkinjuntti T, Pantoni L, Fazekas F, et al. (2010), White matter changes and diabetes predict cognitive decline in the elderly: the LADIS study. Neurology 75:160-167.

Wardlaw JM, Doubal F, Armitage P, Chappell F, Carpenter T, Munoz Maniega S, Farrall A, Sudlow C, et al. (2009), Lacunar stroke is associated with diffuse blood-brain barrier dysfunction. Ann Neurol 65:194-202.

Wardlaw JM, Smith EE, Biessels GJ, Cordonnier C, Fazekas F, Frayne R, Lindley RI, O'Brien JT, et al. (2013), Neuroimaging standards for research into small vessel disease and its contribution to ageing and neurodegeneration. Lancet Neurol 12:822-838.

Wiseman RM, Saxby BK, Burton EJ, Barber R, Ford GA, O'Brien JT (2004), Hippocampal atrophy, whole brain volume, and white matter lesions in older hypertensive subjects. Neurology 63:1892-1897.

Wyss JM, Fisk G, van Groen T (1992), Impaired learning and memory in mature spontaneously hypertensive rats. Brain Res 592:135-140.

Yeatman JD, Wandell BA, Mezer AA (2014), Lifespan maturation and degeneration of human brain white matter. Nat Commun 5:4932.

Yilmaz A, Ulak FS, Batun MS (2004), Proton T1 and T2 relaxivities of serum proteins. Magn Reson Imaging 22:683-688.

Zaharchuk G, Martin AJ, Rosenthal G, Manley GT, Dillon WP (2005), Measurement of cerebrospinal fluid oxygen partial pressure in humans using MRI. Magn Reson Med 54:113-121.

Zhang-James Y, Middleton FA, Faraone SV (2013), Genetic architecture of Wistar-Kyoto rat and spontaneously hypertensive rat substrains from different sources. Physiol Genomics 45:528-538.

Figure1

Click here to download high resolution image

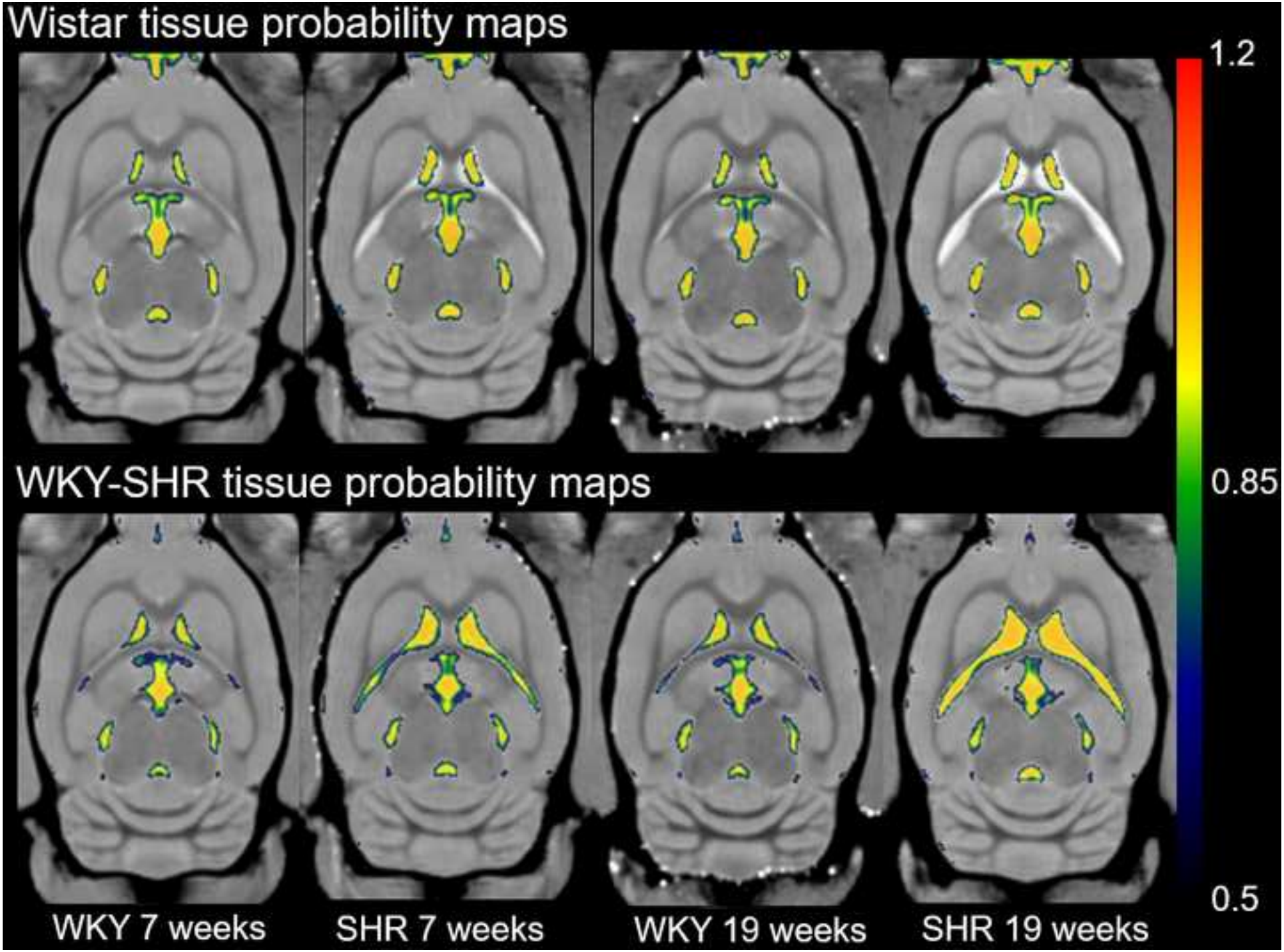

Figure2

Click here to download Figure: Figure2.eps

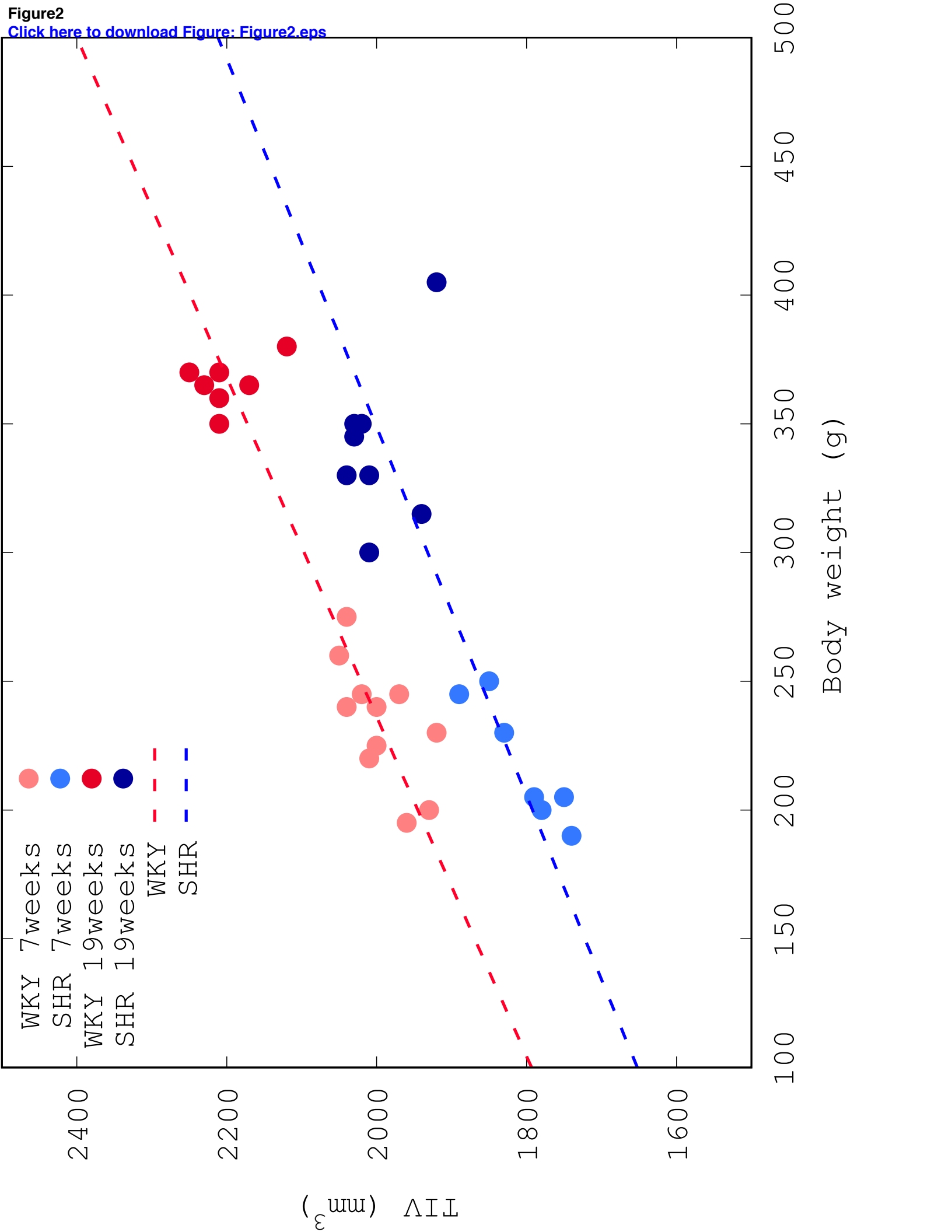

Figure3

Click here to download high resolution image

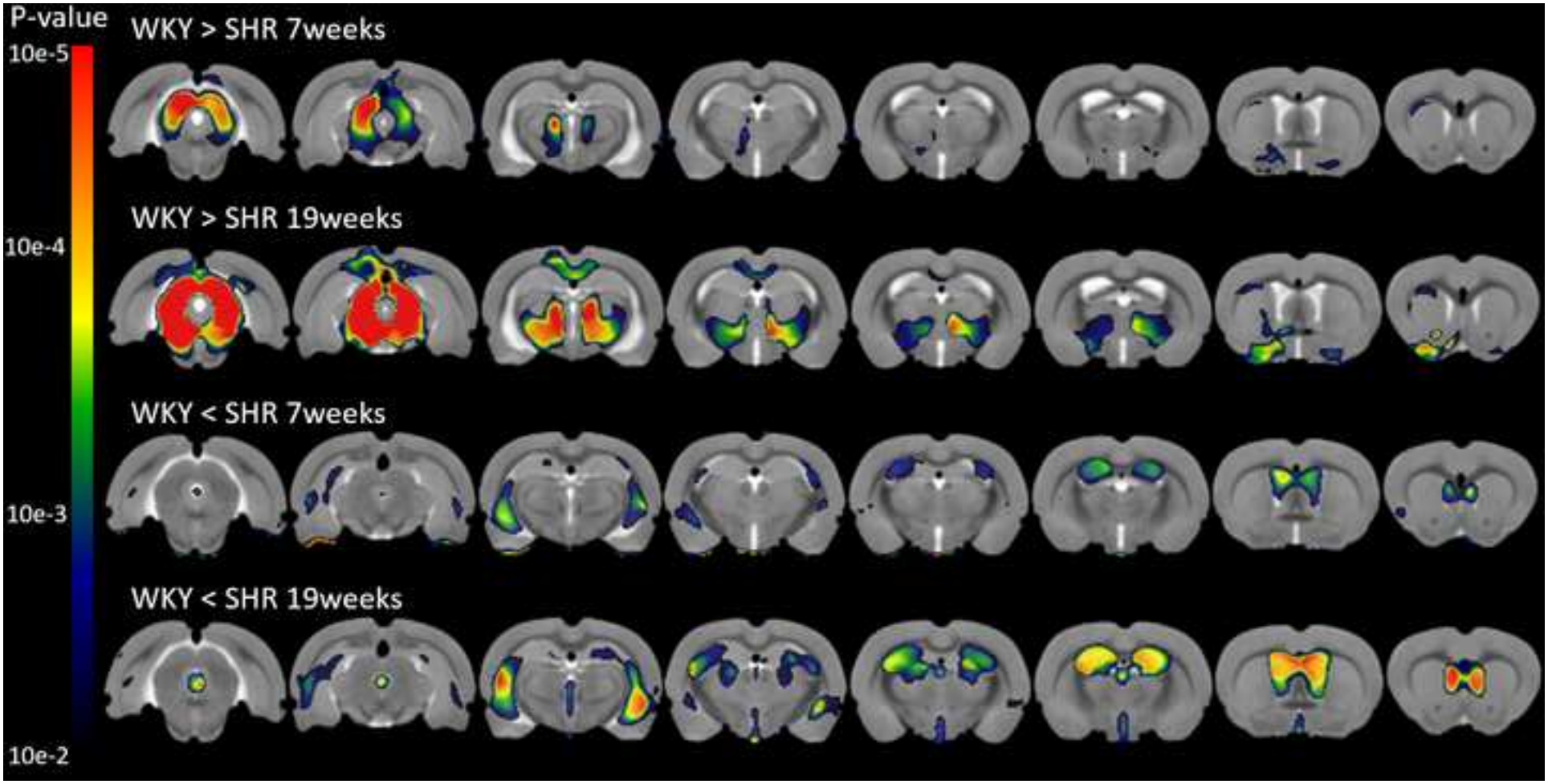

Figure4

Click here to download high resolution image

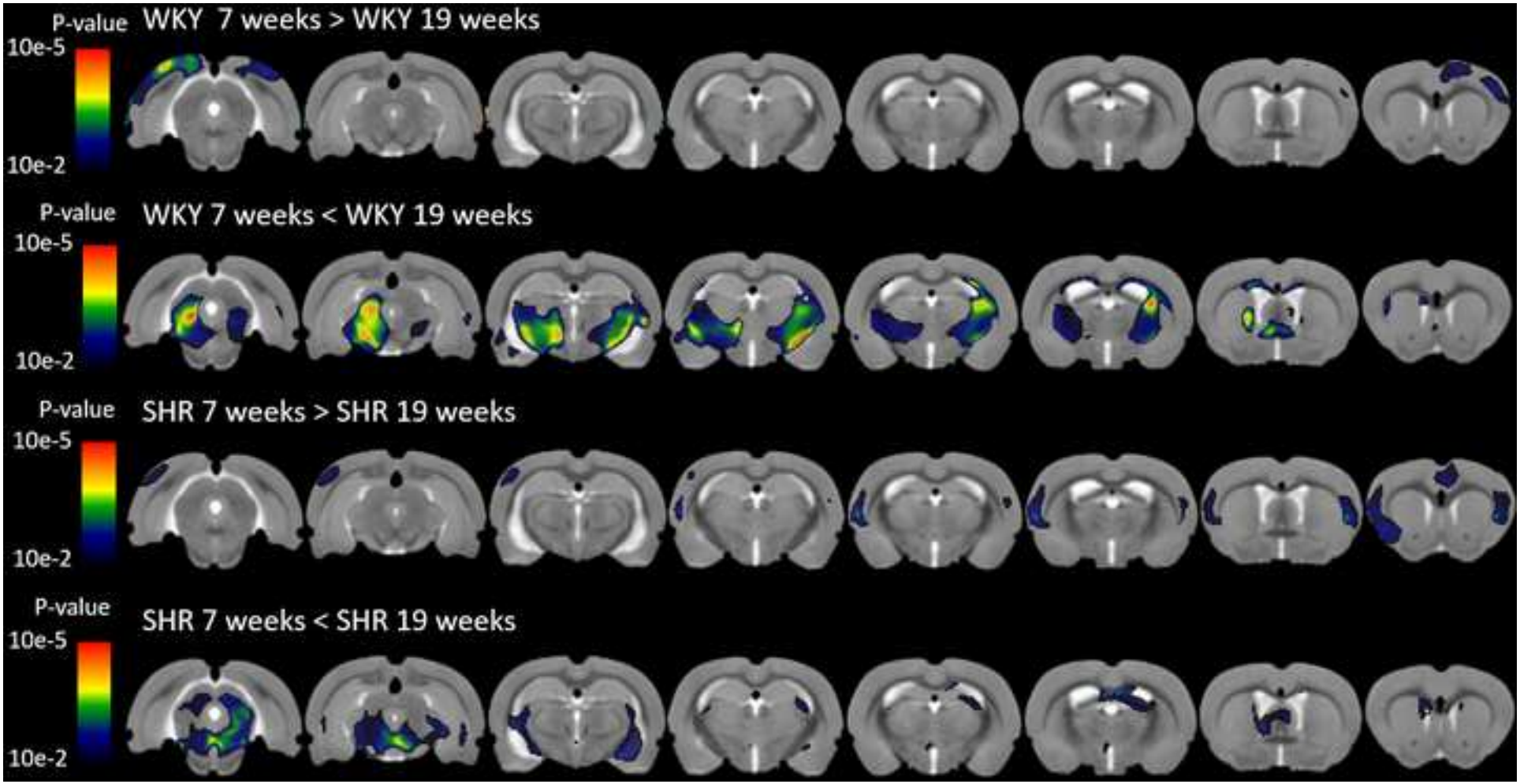

Figure5

Click here to download high resolution image

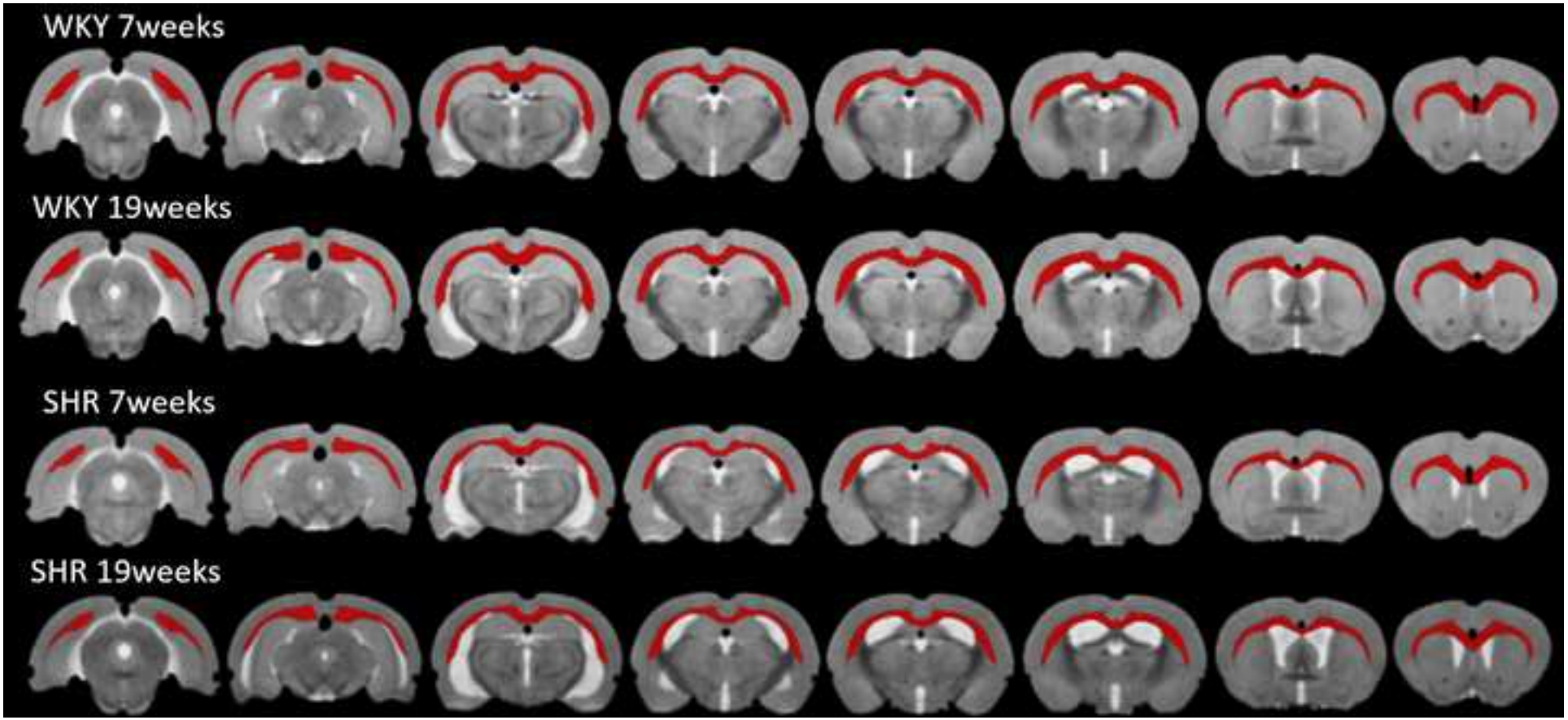

Figure6

Click here to download high resolution image

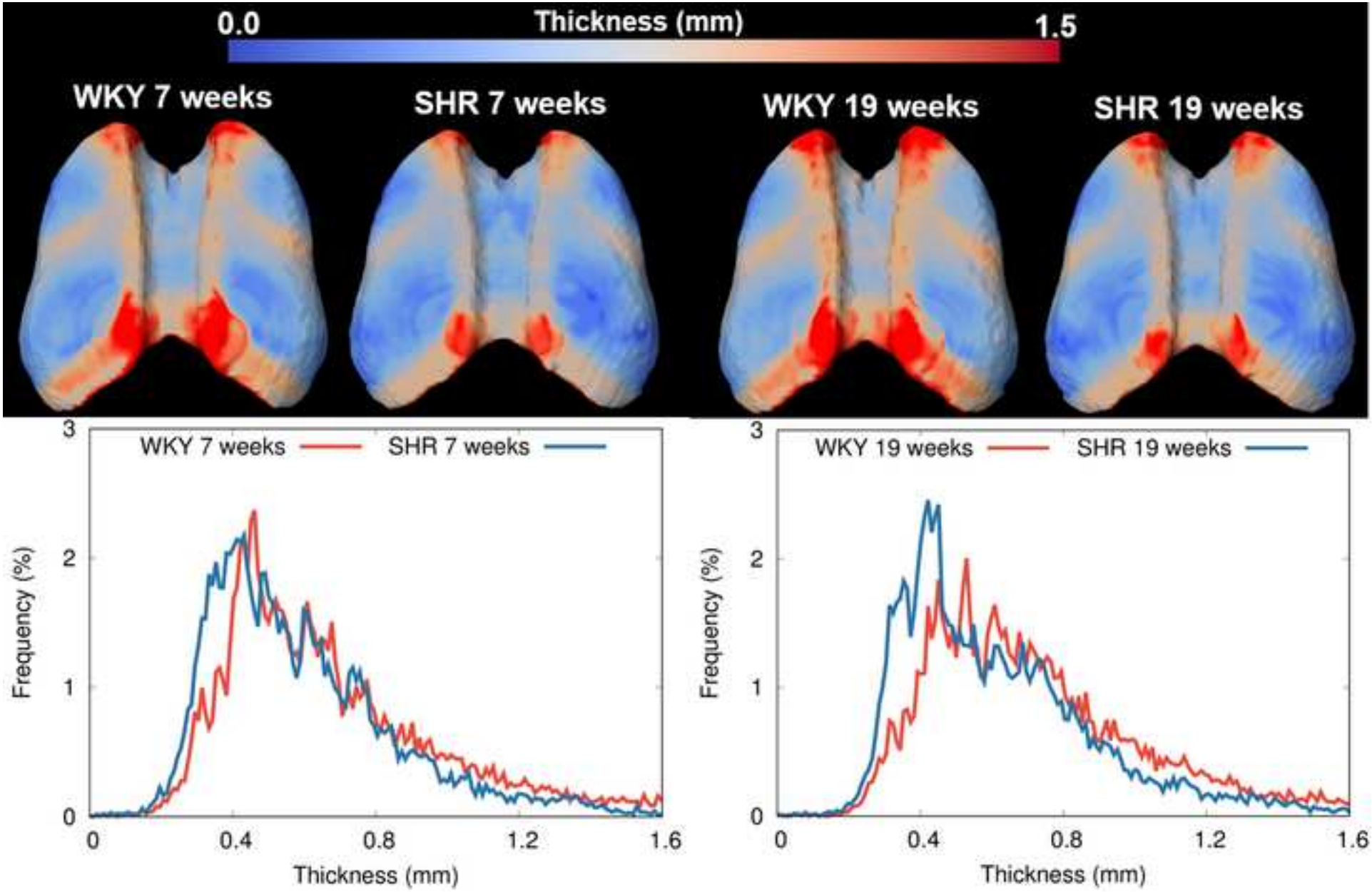

Figure7
Click here to download high resolution image

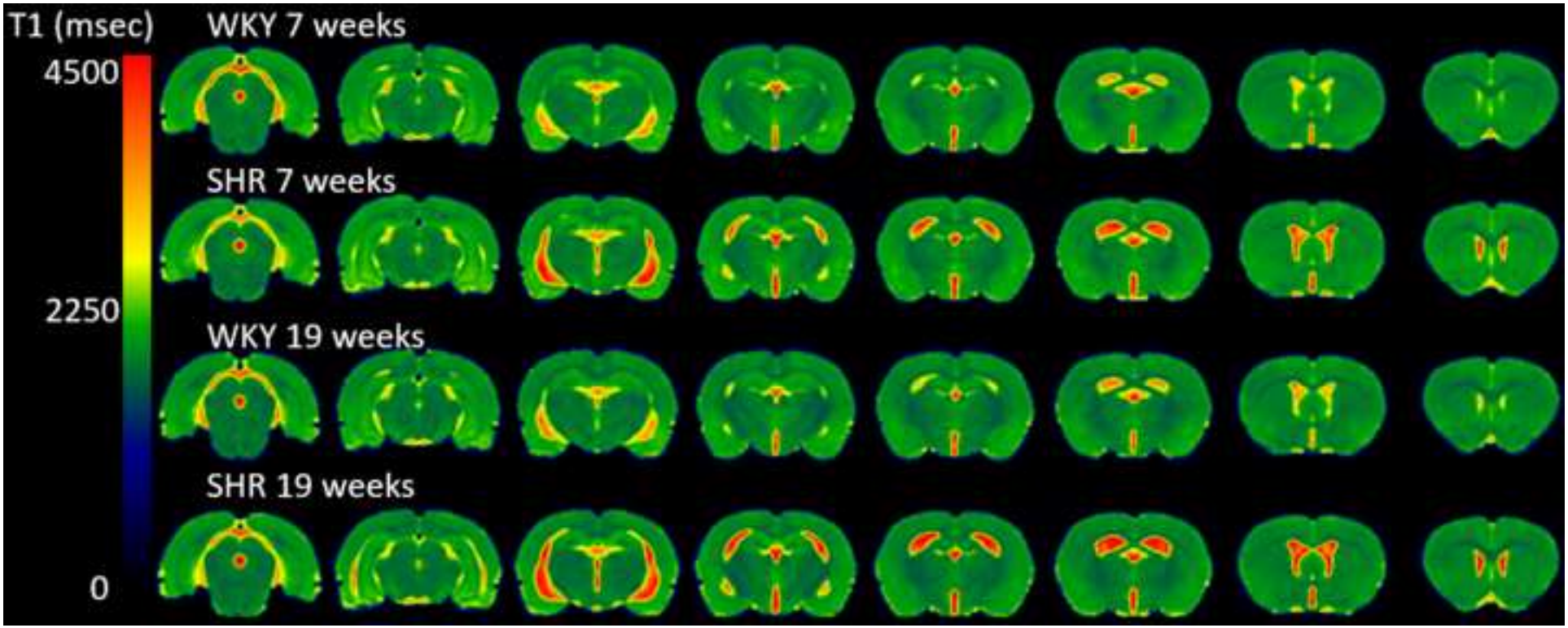

Figure8

Click here to download high resolution image

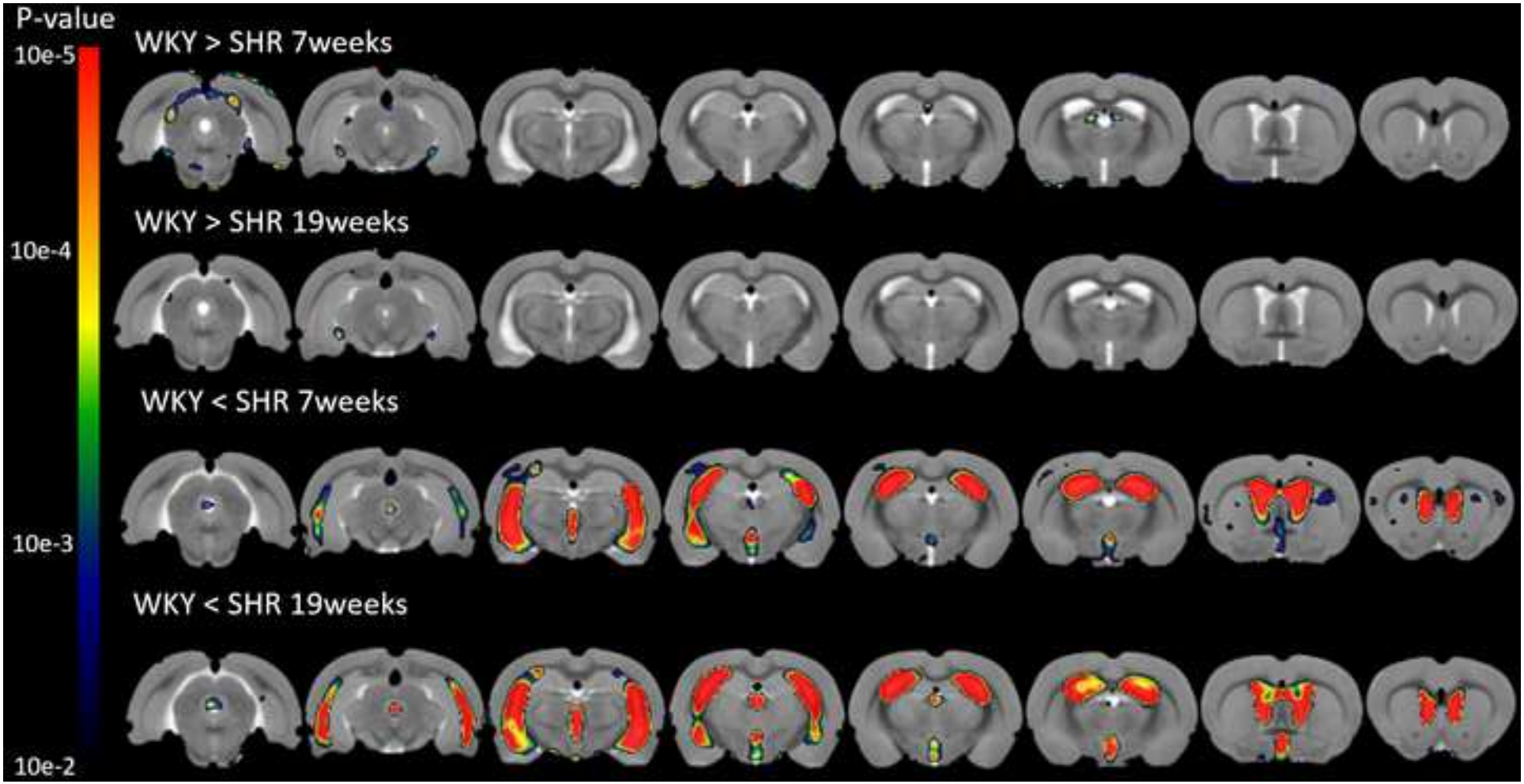

Figure9
Click here to download high resolution image

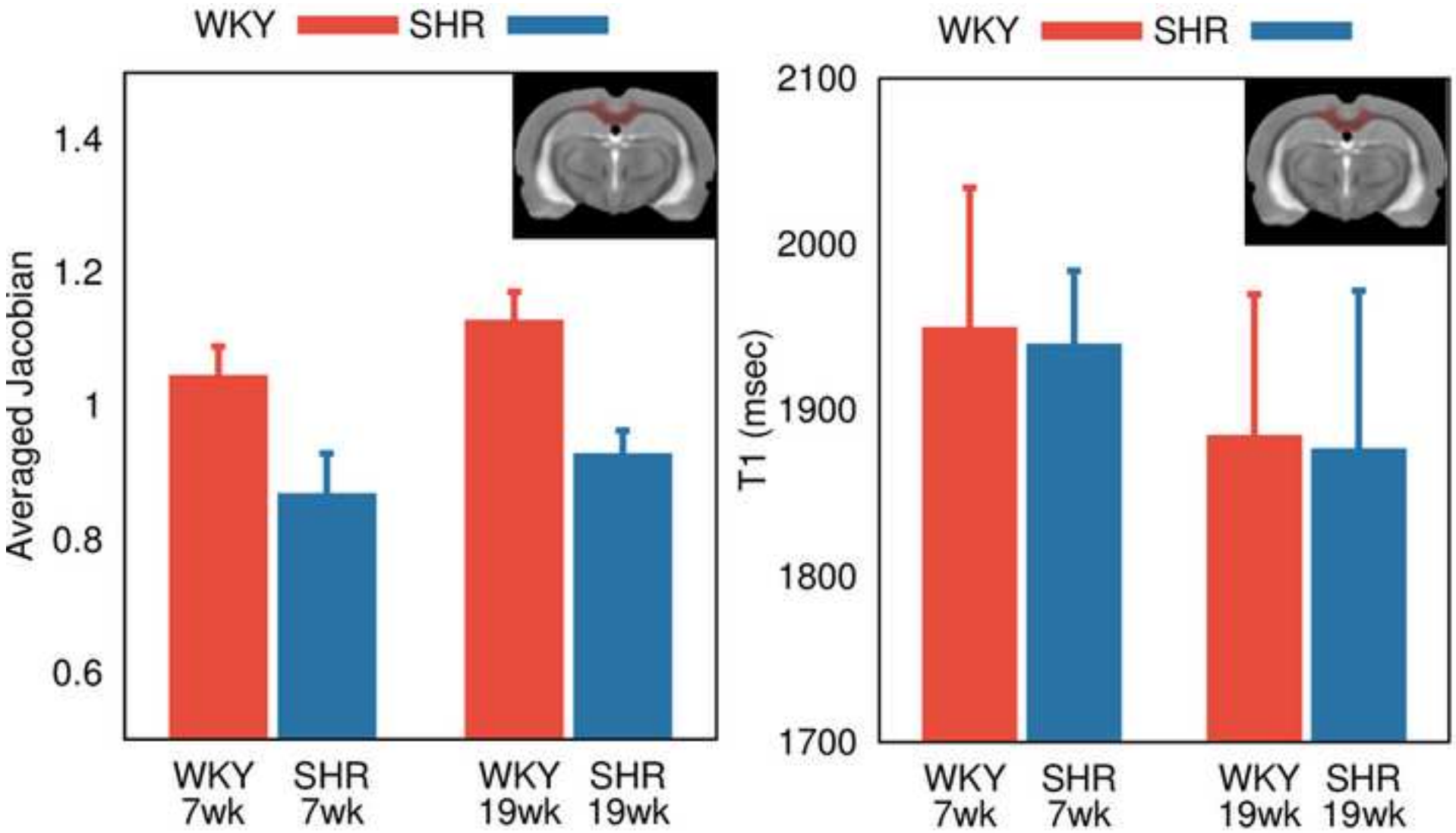

Table

Strain	N	Age (weeks)	GM (mm^3)	WM (mm^3)	CSF (mm^3)	TIV (mm^3)	GM/TIV (%)	WM/TIV (%)	CSF/TIV (%)
WKY	11	7	1112 ± 33	582 ± 21	111 ± 11	1805 ± 36	61.6 ± 1.2	32.2 ± 1.1	6.1 ± 0.6
WKY	8	19	1150 ± 60	675 ± 21	122 ± 11	1946 ± 48	59.0 ± 1.9	34.7 ± 1.4	6.3 ± 0.6
SHR	7	7	1046 ± 35*	473 ± 31*	137 ± 16*	1656 ± 58*	63.2 ± 1.4	28.5 ± 1.3*	8.3 ± 0.9*
SHR	8	19	1094 ± 57*	539 ± 32*	182 ± 17*	1815 ± 37*	60.2 ± 2.3	29.7 ± 2.0*	10.0 ± 1.0*

Table 1. Total grey matter (GM), white matter (WM), and cerebral spinal fluid (CSF) volumes were calculated by the whole brain segmentation method. Volume fractions (%) in each compartment was calculated relative to the total intracranial volumes (TIV). Data are expressed in mean ± SD. * P<0.01 (Tukey post-hoc analysis) compared with the equivalent age group of WKY.

Strain	N	Age (weeks)	Volume (mm^3)	Volume/TIV (%)
WKY	11	7	92.7 ± 3.6	5.1 ± 0.2
WKY	8	19	109 ± 3.5	5.6 ± 0.2
SHR	7	7	76.2 ± 5.8*	4.6 ± 0.2*
SHR	8	19	90 ± 3.2*	5.0 ± 0.2*

Table 2. The corpus callosum volumes were derived using a semi-automated computerized method. Volume fractions (%) were calculated relative to the total intracranial volumes (TIV). Data are expressed in mean ± SD. * P<0.01 (Tukey post-hoc analysis) compared with the equivalent age group of WKY.

Strain	N	Age	GM (msec)	WM (msec)	CSF (msec)	CC (msec)
WKY	11	7	2095 ± 42	1899 ± 43	3274 ± 89	1919 ± 55
WKY	8	19	2078 ± 69	1857 ± 53	3298 ± 222	1881 ± 70
SHR	7	7	2119 ± 52	1898 ± 50	3459 ± 161	1981 ± 48
SHR	8	19	2069 ± 93	1849 ± 63	3676 ± 105*	1934 ± 90

Table 3. Mean and SD of T1 within GM, WM, CSF and corpus callosum. Data are expressed in mean ± SD. * P<0.01 (Tukey post-hoc analysis) compared with the equivalent age group of WKY.